EARTH SURFACE PROCESSES AND LANDFORMS
Earth Surf. Process. Landforms (2014)

Published online in Wiley Online Library
(wileyonlinelibrary.com) DOI: 10.1002/esp.3666

The influence of ground ice distribution on geomorphic dynamics since the Little Ice Age in proglacial areas of two cirque glacier systems

Jean-Baptiste Bosson,[1]* Philip Deline,[2] Xavier Bodin,[2] Philippe Schoeneich,[3] Ludovic Baron,[4] Marie Gardent[2] and Christophe Lambiel[1]

[1] Institut des dynamiques de la surface terrestre, Université de Lausanne, Lausanne, Switzerland
[2] Laboratoire EDYTEM, Université de Savoie, CNRS, Le Bourget-du-Lac, France
[3] Institut de Géographie Alpine, PACTE/Territoire, Université Joseph Fourier, Grenoble, France
[4] Institut des sciences de la Terre, Université de Lausanne, Lausanne, Switzerland

Received 15 August 2013; Revised 13 October 2014; Accepted 14 October 2014

*Correspondence to: Jean-Baptiste Bosson, Institut des dynamiques de la surface terrestre, Université de Lausanne, Lausanne, Switzerland.
E-mail: jean-baptiste.bosson@unil.ch

ESPL
Earth Surface Processes and Landforms

ABSTRACT: Holocene glaciers have contributed to an abundance of unstable sediments in mountainous environments. In permafrost environments, these sediments can contain ground ice and are subject to rapid geomorphic activity and evolution under condition of a warming climate. To understand the influence of ground ice distribution on this activity since the Little Ice Age (LIA), we have investigated the Pierre Ronde and Rognes proglacial areas, two cirque glacier systems located in the periglacial belt of the Mont Blanc massif. For the first time, electrical resistivity tomography, temperature data loggers and differential global positioning systems (dGPS) are combined with historical documents and glaciological data analysis to produce a complete study of evolution in time and space of these small landsystems since the LIA. This approach allows to explain spatial heterogeneity of current internal structure and dynamics. The studied sites are a complex assemblage of debris-covered glacier, ice-rich frozen debris and unfrozen debris. Ground ice distribution is related to former glacier thermal regime, isolating effect of debris cover, water supply to specific zones, and topography. In relation with this internal structure, present dynamics are dominated by rapid ice melt in the debris-covered upper slopes, slow creep processes in marginal glacigenic rock glaciers, and weak, superficial reworking in deglaciated moraines. Since the LIA, geomorphic activity is mainly spatially restricted within the proglacial areas. Sediment exportation has occurred in a limited part of the former Rognes Glacier and through water pocket outburst flood and debris flows in Pierre Ronde. Both sites contributed little sediment supply to the downslope geomorphic system, rather by episodic events than by constant supply. In that way, during Holocene and even in a paraglacial context as the recent deglaciation, proglacial areas of cirque glaciers act mostly as sediment sinks, when active geomorphic processes are unable to evacuate sediment downslope, especially because of the slope angle weakness. Copyright © 2014 John Wiley & Sons, Ltd.

KEYWORDS: proglacial area; permafrost; glacier–permafrost interaction; debris-covered glacier; ground ice; sediment transfer system

Introduction

Glacier shrinkage, initiated at the end of the Little Ice Age (LIA: AD 1300–1850/60 in the Alps; Ivy-Ochs *et al.*, 2009) and accelerated since the mid 1980s, has led to the rapid growth of many proglacial areas worldwide (Vaughan *et al.*, 2013). These recently deglaciated areas are incredibly dynamic and rapidly changing as a result of intensive paraglacial readjustment and high sediment flux (Ballantyne, 2002; Meigs *et al.*, 2006; Otto *et al.*, 2009; Carrivick *et al.*, 2013). Proglacial areas have a key role in the sediment cascade systems in mountainous environments (Geilhausen *et al.*, 2012). As a function of their ability to transfer sediment load downslope, they can act 'either as a sink or as a source of sediment' (Owens and Slaymaker, 2004, p. 15).

In high relief and permafrost environments, proglacial areas may have one or both of two characteristics in relation with sediment flux. First, there may be thick moraine accumulations. Repeated Holocene fluctuations of heavily debris-covered glaciers can result in the formation of moraine ramparts (also called dams, dumps or bastions: Shroder *et al.*, 2000; Benn *et al.*, 2003; Hambrey *et al.*, 2008). These landforms are especially common in flatter terrain dominated by high rock walls, such as cirques or valley floors inherited from the last Pleistocene glaciation, where the linkage between the glacial and the hydrological transport systems is inefficient (Benn *et al.*, 2003). Second, there may be strong glacier–permafrost interactions. As a consequence of development of polythermal glacier systems within the periglacial belt (Cuffey and Paterson, 2010) and of ice recession, massive ice, ice-cemented and ice-free sediments may coexist in proglacial areas (Reynard *et al.*, 2003; Haeberli, 2005; Kneisel and Kääb, 2007; Ribolini *et al.*, 2010). As shown by examples in mountainous and polar regions, glacier

oscillations in permafrost environments may form complex marginal sediment accumulations that contain ice, such as rock glaciers, push moraines, and ice cored moraines (Brazier *et al.*, 1998; Owen and England, 1998; Serrano and López-Martínez, 2000; Krainer and Mostler, 2006; Lilleøren *et al.*, 2013). The distribution of ground ice in these environments appears to be ambivalent in relation to sediment flux (Gomez *et al.*, 2003; Etzelmüller and Hagen, 2005; Kääb *et al.*, 2005; Chiarle *et al.*, 2007; Huggel *et al.*, 2011). It can both increase flux, by encouraging the sliding, deformation and/or melting of the frozen zone, and by acting as an aquiclude layer or a sliding plane; but also limit, by sediment cementation, the transfer process.

In addition to the difficulties of field investigations in high mountain environments, the development of appropriate methods to study the internal structure (e.g. boreholes, geophysical prospections) and surface dynamics (e.g. differential global positioning system (dGPS), photogrammetry, terrestrial laser scanning) of proglacial areas is only quite recent. Although research in this area has developed rapidly over the last 15 years (see e.g. Kneisel, 1999; Delaloye, 2004), knowledge remains sparse. Existing studies have mainly focused on the current distribution of ground ice and/or geomorphic activity. Detailed analyses of post-LIA evolution are few, and characterization of the internal structure, using geophysics or boreholes, has been restricted to small parts of former glacier systems. Deglaciation and its influence on current ground ice distribution, ice/sediment volumes, active geomorphic processes, and sediment flux rates are topics that are still largely unknown. Complete temporal and spatial geomorphic analysis of proglacial areas in mountainous permafrost environments remains a challenging task. Such a complete study would also allow the identification of the specificities of these complex landforms in sediment transfer systems in comparison with other proglacial areas.

This paper aims to quantify for two small neighbouring Alpine sites in the periglacial belt of the Mont Blanc massif how the ground ice that remains following deglaciation has impacted upon geomorphic processes since the LIA. Our study combines several methods for internal structural characterization (electrical resistivity tomography, ground surface temperature measurements) and surface evolution analysis over various timescales (dGPS survey, geomorphological mapping, historical documentation).

Study Sites

The Rognes and Pierre Ronde areas (45°51′38″N, 6°48′40″E; 2600–3100 m above sea level (a.s.l.)) are two cirque glacier systems located north of the Bionnassay Glacier basin, in the French part of the Mont Blanc massif (Figures. 1 and 2). The lithology comprises micaschists and mylonitized gneiss of the Mont-Blanc external units (Mennessier *et al.*, 1976). Intense rockfalls affect the surrounding rockwalls, explaining the frequent extended debris cover on local glaciers (Deline, 2005). The northwest part of the Mont Blanc massif acts as a topographic barrier for the dominant westerly humid air masses. This partly explains why the local glaciers have experienced slower recession than others in the French Alps (Gardent *et al.*, 2014). Because of this humidity, Holocene glacial morphodynamics prevails in the massif, and periglacial landforms such as rock glaciers are relatively uncommon (Bosson, 2012). Extrapolated from Krysiecki *et al.* (in preparation) and Gilbert *et al.* (2012), the current mean annual air temperature (MAAT) at the Rognes shelter (2768 m a.s.l., Figures 1 and 2) is −0.9 °C and the average annual precipitation is *c.* 2000 mm. Since the 1990s, the local mean glacier equilibrium-line altitude (ELA) has fluctuated around 3200 m a.s.l. (Gilbert *et al.*, 2012), *c.* 100 m above the studied sites. The local lower limit of the

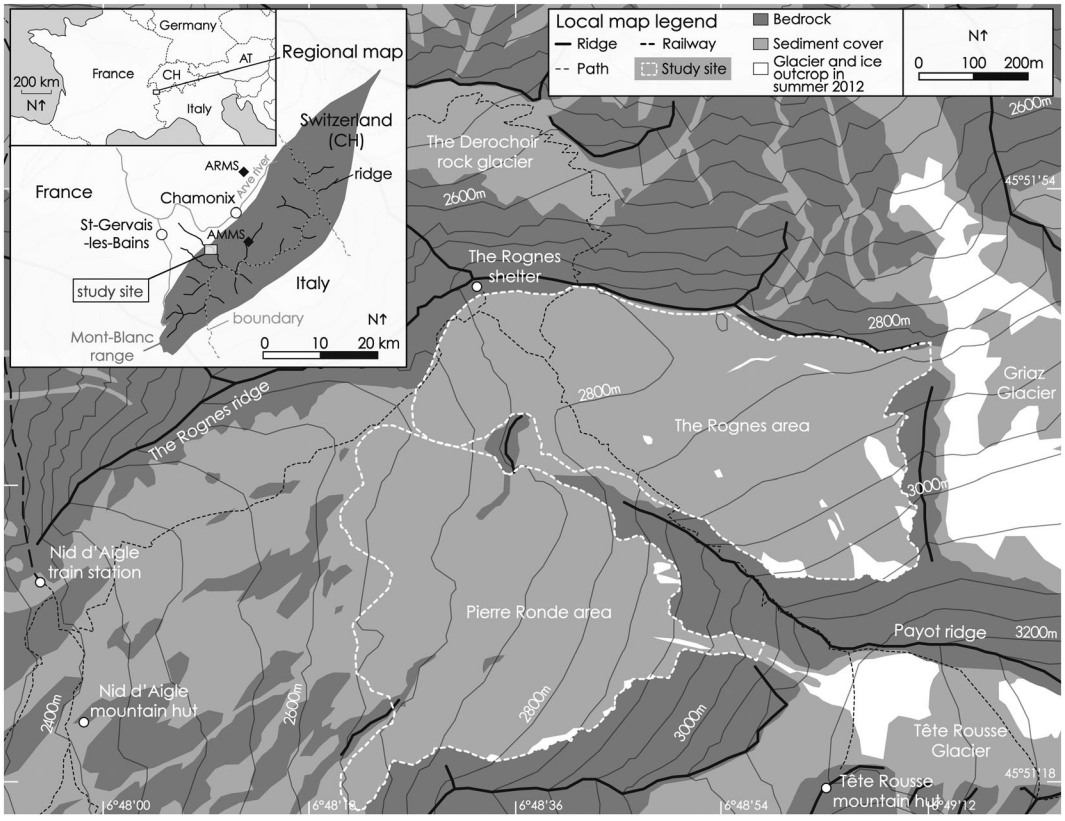

Figure 1. Location and topography of the Rognes and Pierre Ronde areas. AMMS and ARMS: Aiguille du Midi and Aiguilles Rouges weather stations, respectively.

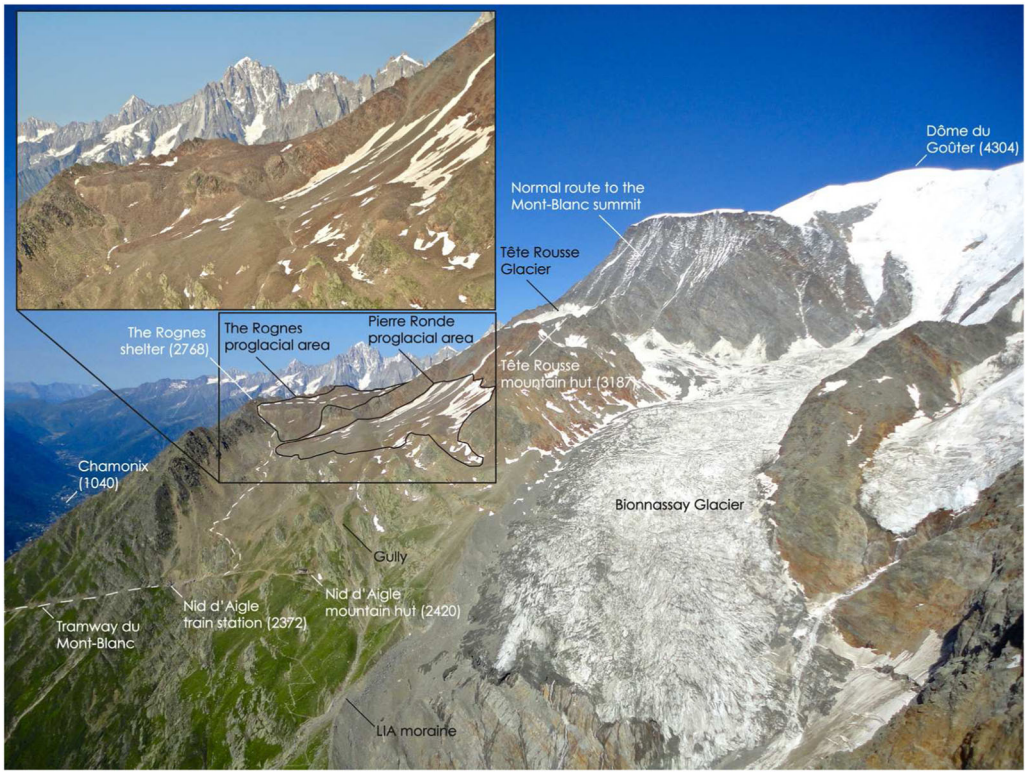

Figure 2. Upper Bionnassay Glacier basin seen from the Tricot ridge (photograph by D. Bonneaux, July 2012). This figure is available in colour online at wileyonlinelibrary.com/journal/espl

periglacial belt is close to 2450 m a.s.l. as indicated by the nearby active Dérochoir rock glacier (Krysiecki *et al.*, in preparation).

Whereas many glaciological data exist for the local glaciers (e.g. Bossons, Tête Rousse, Taconnaz), the Pierre Ronde and Rognes areas have never been studied. Historical documents, such as post-1860s maps, give imprecise and contradictory information on glacier extents at these sites. Today, the Rognes and Pierre Ronde are two small vanishing debris-covered cirque glaciers. They dominate a sediment area bounded downstream by a steep 25- to 40-m-high talus. The steepness of the foreslope and the absence of noticeable vegetation cover suggest recent glacier recessions and active post-glacial dynamics.

The Rognes system (0.29 km^2, 2650–3100 m a.s.l.) lies in a small cirque floor oriented north-northwest, that appears filled by sediments (Figures 2 and 3). A debris-covered slope with few ice outcrops dominates a depressed area with marginal, rounded sediment ridges. The glacier front is hidden, except on the north side, where a 0.5–1-m-high vertical rim and an ice cave expose glacier limits (Figure 3C). During the LIA, the north branch of the Rognes Glacier was connected to the Griaz Glacier and flowed into the Chamonix valley, whereas the main northwest branch is located in the Bionnassay basin.

The Pierre Ronde system (0.28 km^2, 2600–3000 m a.s.l.) occupies a small northwest-facing cirque floor below the Tête Rousse trough (Figures 1 and 3). A talus slope with some ice outcrops overlooks a depression in which the limits of the glacier are invisible. Gullies and fresh deposits illustrate debris flow activity in the last few years; the last major event mobilized *c.* 10 000 m^3 of sediments in September 2009 (B. Demolis, Service Restauration des terrains en montagne of Haute-Savoie, personal communication). In the distal part, the smoothed fine sediments on the west contrast with the coarse accumulation with ridges and furrows on the north. The Pierre Ronde Glacier was connected to the Tête Rousse Glacier by an ice couloir during the LIA. In 1892, a major water-pocket outburst flood (WPOF) occurred; 200 000 m^3 of water and ice hurtled down this couloir and travelled across Pierre Ronde, where a part of the till cover was mobilized. The debris flow of 800 000 m^3 covered a distance of 14 km and devastated

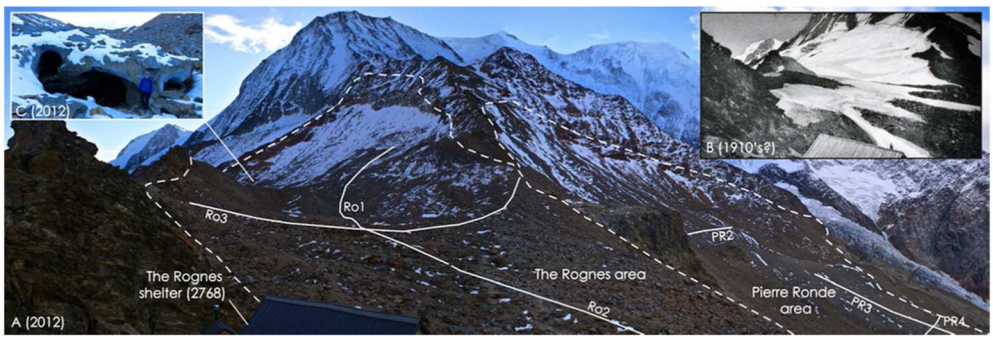

Figure 3. View of the upper area of Rognes taken from the same location on October 2012 (A, photograph S. Utz) and probably in the 1910s (B, CNM collection). Dotted lines: studied area limits; solid lines: ERT profiles. (C) Ice cave in the north distal part of the Rognes area (location in Figure 8). This figure is available in colour online at wileyonlinelibrary.com/journal/espl

the village of Saint-Gervais-les-Bains, causing 175 fatalities (Vincent *et al.*, 2010). Because of the development of cold ice at the base of Tête Rousse Glacier snout since 1980s, a new sub-glacial lake has formed (Gilbert *et al.*, 2012; Vincent *et al.*, 2012). To prevent further WPOFs, water has been pumped each summer since 2010. As well, an important amount of unconsolidated sediment in Pierre Ronde could be mobilized with a new WPOF.

Methods

Field data were collected in 2011 and 2012 to detect the current distribution of ground ice and to understand its origin and influence on geomorphic dynamics.

Geoelectrical survey

Because of the contrast between ice (resistive) and water (conductive, Figure 4), electrical resistivity tomography (ERT) is a commonly used method in permafrost and ground ice investigation (e.g. Hambrey *et al.*, 2008; Hauck and Kneisel, 2008; Ribolini *et al.*, 2010; Scapozza, 2013). Apparent resistivity is measured along transects between *n* pairs of electrodes installed at the ground surface. A plausible image of the specific resistivity of subsurface layers is modelled through an inversion process and repeated iterations.

In Summer 2012, 5 m inter-electrode spacing ERT profiles were measured at Rognes and Pierre Ronde, leading to two 24*e* (i.e. electrodes), three 48*e*, one 60*e* and one 120*e* profiles (Figures 3 and 5). Apparent resistivities were measured with a Syscal Pro Switch 96 with a Wenner–Schlumberger configuration, the latter being chosen because it represents a good compromise between horizontal resolution and depth of investigation. We improved the electrodes-sediments contact with salt-water saturated sponges. Results were treated with Prosys II (Iris Instruments, Orleans, France), taking into account the surface topography measured with dGPS. The inversion was processed with Res2DInv, based on least-squares inversion and robust parameters (which allow a good visualization of high resistivity contrasts) with the following parameters: initial damping factor =0.15; minimum damping factor =0.02; vertical to horizontal flatness filter ratio =1; (robust) cutoff factor for data constrain =0.05; (robust) cutoff factor for model constrain =0.005. Final tomograms express the plausible ground resistivities with absolute error corresponding to the difference in percentage between inverted model and measured data. To evaluate the reliability of the inverted model and distinguish regions that are well constrained by measured data to those that could correspond to inversion artefacts, we produced a model resolution matrix analysis (see details in Stummer *et al.*, 2004; Hilbich *et al.*, 2009). The model resolution matrix value (MRMV) compares modelled values with measured values: the better modelled and measured values fit, the closer to one the MRMV. MRMV is a function of ground conductivity, and decreases rapidly with depth in highly resistive zones (Figure 5; Hilbich *et al.*, 2009). We have displayed the thresholds of 0.05 and 0.005 MRMV in our tomograms and considered regions with MRMV >0.05 as reliable, regions with MRMV >0.005 as moderately to weakly reliable, and regions with MRMV <0.005 as only very weakly reliable.

Ground surface temperature (GST) measurements

In order to obtain quantitative indicators of the thermal state of the ground surface and of the possible presence of ground ice close to the surface, a network of 18 miniature temperature sensors (IButton DS1922L, accuracy of 0.065 °C) was set up at the near ground surface, shielded from direct solar radiation (see Figure 6 for location). Temperature was sampled at a two hour frequency for all sensors between 10 September 2011 and 20 June 2012. Mean ground surface temperature (MGST) for the measurement period, ground freezing index (GFI, i.e. sum of negative mean daily temperatures) and winter equilibrium temperature (WEqT; Delaloye, 2004) were calculated. As ground surface is an interface layer, influenced by the ground and the atmosphere, these climatic parameters (calculated for the nine coldest months of a year in this study) give interesting and complementary information on the ground thermal state and on the possible occurrence of ice near the surface. Negative MGST values may indicate an influence of cold ground thermal regime (related to ice occurrence and/or cold air trapping in the interstices) and/or cold topoclimatic conditions. In this way, ground ice is more likely to exist and to persist under the coldest negative MGST. GFI estimates the 'amount of cold' stored in the ground during the frozen days. Finally, WEqT is reached when a significant snow cover isolates the ground from atmospheric influence and temperature tends to an equilibrium controlled by the heat transfer from the upper ground layers. Cold WEqT values (some degree below 0 °C) possibly indicate an influence of ground ice or permafrost conditions in the ground.

In addition, mean daily temperature curves were displayed for each sensor to characterize the ground surface thermal regime and its relation to air temperature and snow cover. We present the daily temperature curves of four sensors (three sensors along a longitudinal profile in Rognes and the sensor located in Pierre Ronde, see Figure 6B) in parallel with air temperature at Aiguille du Midi weather station (AMMS in Figure 1;

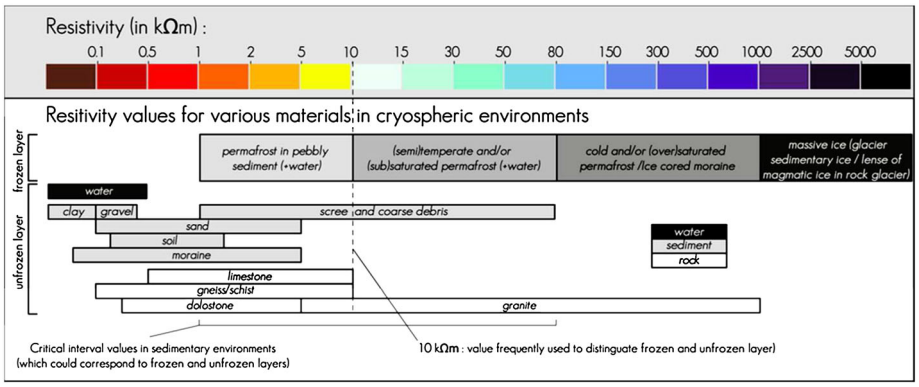

Figure 4. Resistivity scale used in this study and typical values of various materials. Adapted from Hauck and Kneisel (2008) and Scapozza (2013). This figure is available in colour online at wileyonlinelibrary.com/journal/espl

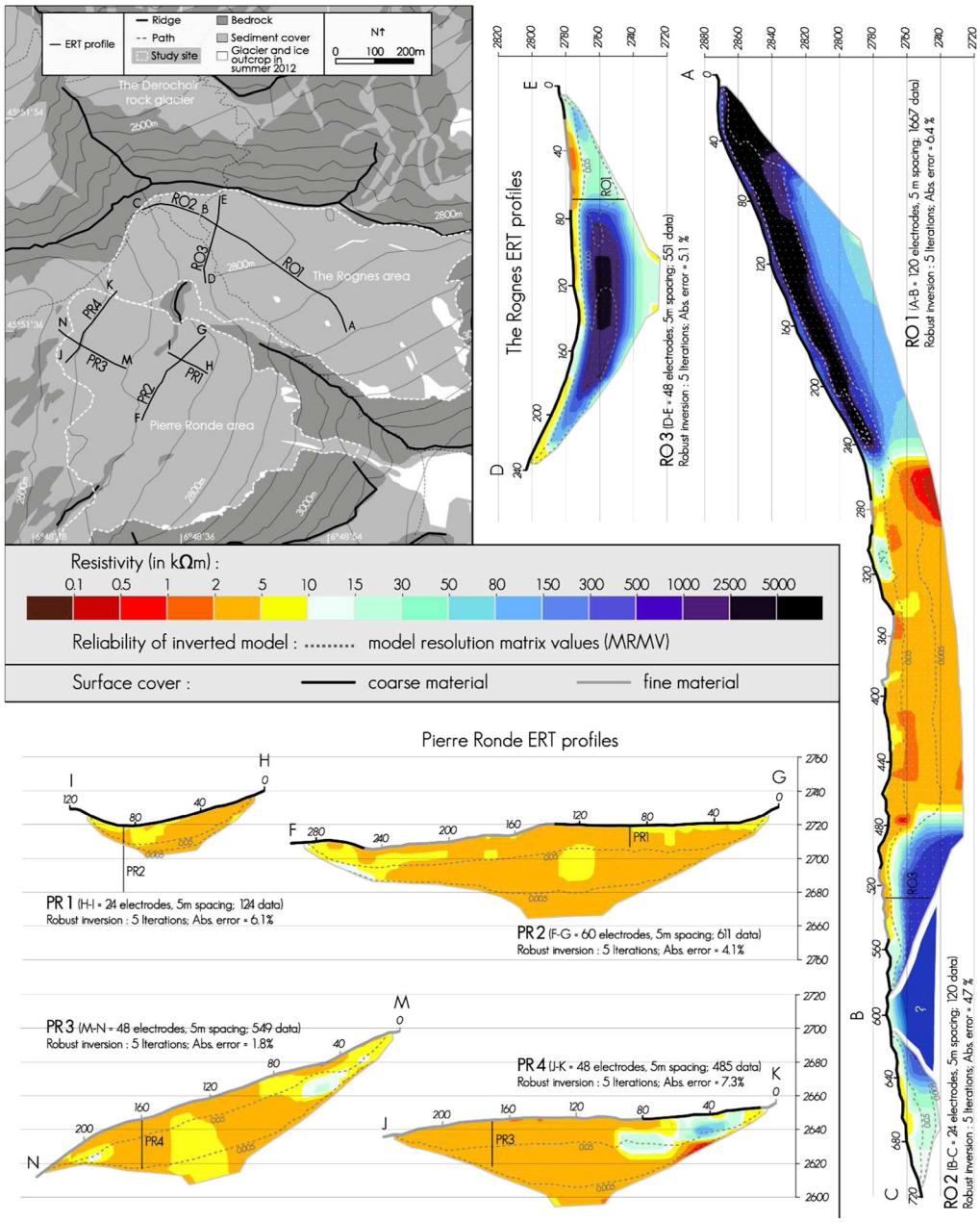

Figure 5. Transversal and longitudinal electrical resistivity tomograms obtained in Rognes and Pierre Ronde areas on 28 and 29 August 2012. This figure is available in colour online at wileyonlinelibrary.com/journal/espl

at 3845 m a.s.l. and 6 km distant of study sites, Météo France data) and the snow cover thickness at the Aiguilles Rouges weather station (ARMS in Figure 1; at 2330 m a.s.l. and 15 km distant of study sites, Météo France data).

Results from ground temperature measurements have to be considered carefully. They vary strongly in time and space and rarely allow the definitive identification of permafrost and/or ground ice occurrence (Delaloye, 2004). They are qualitative indicators (thermal state of the ground during a specific period, possibility of permafrost and/or ground ice occurrence, local cold/warm area repartition) rather than quantitative in order to characterize the ground.

Differential global positioning system (dGPS) measurements

The position of 63 boulders in Rognes and 24 boulders in Pierre Ronde were measured with a Leica SR500 in September 2011 and 2012, and in July and October 2012, respectively. Both vertical (Vm) and horizontal (Hm) movements were computed, with a precision of ±5 cm.

Following Lambiel and Delaloye (2004), we assume that in ground ice sedimentary environments, the measured vertical component of the movement corresponds to a possible combination of three main processes: (1) loss in elevation consecutive to the downslope movement along inclined bed, which depends directly on the horizontal component and the slope angle; (2) change in elevation relative to extending and compressing flow; and (3) change in elevation relative to variation of ice volume (local gain or loss of ice). Compressing and extending flows are difficult to point out in our field sites and are assumed to be secondary in the time study window (three months for Pierre Ronde, one year for Rognes). In this way, we calculated the difference (Δv) between the measured vertical component and the expected downslope vertical component (calculated for each point from the measured horizontal component and topographical slope obtained with a 4 m resolution digital elevation model (DEM)). Thus, we assume that Δv can be interpreted as a marker of ice volume variation.

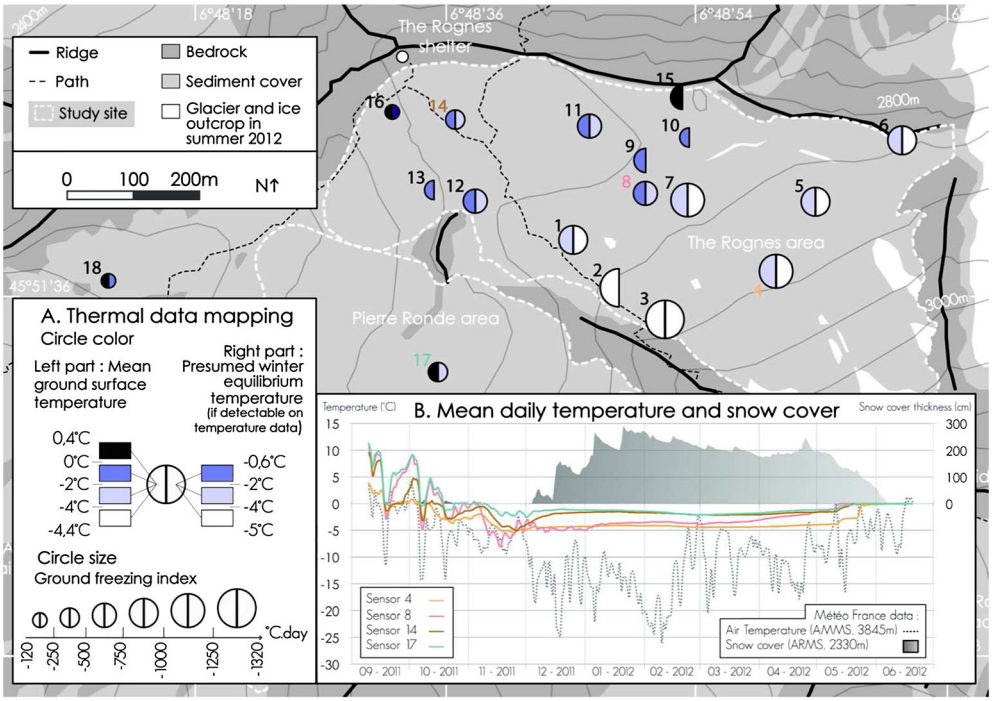

Figure 6. (A) Mean ground surface temperature (MGST), presumed winter equilibrium temperature (WEqT), and ground freezing index (GFI) obtained at 18 locations with ground surface temperature measurements between 10 September 2011 and 20 June 2012 at Rognes and Pierre Ronde. For sensors 2, 9, 10, 13 and 15, the important variability of winter temperatures (probably due to a thin snow cover) did not allow the winter equilibrium temperature to be determined. (B) Mean daily temperature of sensors 4, 8, 14, 17 and air at the Aiguille du Midi weather station (AMMS), and snow cover thickness at Aiguilles Rouges weather station (ARMS) between 10 September 2011 and 20 June 2012 (Météo France data). This figure is available in colour online at wileyonlinelibrary.com/journal/espl

Geomorphological analysis

Finally, critical and comparative analyses of field measurement results, field observations and historical documents (Table I and Figure 3B) were used to provide a global insight on current internal structure and geomorphic dynamics and their evolution since the LIA.

To go beyond the controversy over rock glacier origins, and because high altitude cryospheric landforms can generally be thought as a complex continuum where massive and interstitial ice can coexist, we grouped glacial and periglacial landforms together in our map legend. We term rock glacier a complex, deformed, sediment accumulation with ground ice, steep front with fine material, and ridges and furrows in coarse sediment surface like the Rognes frozen marginal zone or the upper south side of Pierre Ronde. Types of rock glaciers have been discerned according to sediment origin (debris versus talus rock glacier; Barsch, 1996).

Based on the literature, field observations (front thickness of sediment accumulation, surface topography and morphology, bedrock outcrops) and ERT results, sediment volume was approximated. The sediment/ice ratio in the frozen coarse blocky zone was extrapolated from existing literature (Barsch, 1996; Burger *et al.*, 1999; Haeberli *et al.*, 2006; Hausmann *et al.*, 2007; Otto *et al.*, 2009; Scapozza, 2013) and ERT results: we used the value of 30% of sediment content for complex landforms derived from the glacier system (debris rock glaciers) and 60% of sediment content for the almost inactive talus rock glacier of Pierre Ronde. The rough estimation of sediment volume was simply calculated with:

- For unfrozen sediment accumulation: $\mathrm{Vs} = AT$ (1)
- For frozen sediment accumulation: $\mathrm{Vs} = At + A(T-t)C$ (2)

where Vs is the estimated sediment volume, A is the area of sediment accumulation, T is the mean estimated sediment thickness, t is the mean estimated unfrozen surface layer thickness of frozen accumulation and C the estimated sediment content in frozen accumulation.

Results and Interpretation

Electrical resistivity tomography (ERT) profiles

Two sectors were investigated in Pierre Ronde (Figures 3 and 5). In the upper area (2740–2710 m a.s.l.), a short 24*e* longitudinal profile (PR1: H–I) extends from the distal part of the talus slope to a small topographical hump probably related to bedrock. PR1 cuts PR2 (F–G), a 60*e* (a 48*e* profile partially overlaid with a 24*e* profile) transverse profile which crosses the central depression and the fresh debris flow deposits. In the lower area (2700–2610 m a.s.l.), PR3 (M–N, 48*e*) is a longitudinal profile in the west smooth fine sediments, whereas PR4 (J–K, 48*e*) is a transverse profile that crosses the whole sediment area from the coarse and wrinkled northeast to the fine southwest.

With resistivity mostly in the range 2–5 kΩm (with patches of material in the range 5–10 kΩm), conductive materials dominate all tomograms in the whole depth of investigation (up to 40 m for PR2, PR3 and PR4). The good penetration of electric current in this conductive ground is expressed by the MRMV >0.05 in the first 10 m deep. In PR2 and PR3, zones with resistivity in the range 10–30 kΩm are visible at 10–15 m depth. In PR4, a 60 m large and 20 m deep sector with resistivities comprised between 10 and 150 kΩm is located under the coarse and wrinkled surface on the northeast side. Except for this zone, there is no specific link between variation of ground resistivity and grain size at the surface. Intersections of PR1–PR2 and PR3–PR4 show a good correspondence between tomograms.

Three profiles were carried out in the Rognes area (Figures 3 and 5). RO1 is a 600 m longitudinal profile of 120*e* (A–B, superposition

Table I. Main historical documents used in this study

Date	Title	Type	Author	Scale	Source
1865	Massif du Mont Blanc	Map	J.J. Mieulet	1:40 000	www.savoie-archives.fr
1876	Le Massif du Mont Blanc	Map	E. Viollet-le-Duc	1:40 000	Frey (1988)
1892 (?)	Limites de la zone affectée par la vidange de la poche d'eau du glacier de Tête Rousse	Map	P. Mougin (?)	?	—
1896	La chaîne du Mont Blanc	Map	A. Barbey, X. Imfeld and L. Kurz	1:50 000	http://imagebase.ubvu.vu.nl/cdm/ref/collection/krt/id/2837
1900s (?)	Les Rognes – Chalet Forestier	Photograph (postcard)	N. Allantaz	—	—
1910s (?)	Le glacier des Rognes (fig. 4)	Photograph	Anonymous	—	Centre de la Nature Montagnarde (Sallanches) collection
1920s (?)	Chemin de fer du Mont-Blanc conduisant au Glacier de Bionnassay (2800 m). N°655	Photograph (postcard)	L. Morand	—	—
1939	Massif du Mont-Blanc. Région du Sud-Ouest	Map	C. Vallot and E. de Larminat	1:50 000	—
1949	IGNF_PVA_1-0__1949-09-04__C3630-0121_1949_F3630-3631_0044	Aerial photograph	IGN	1:23 430	http://www.geoportail.gouv.fr/accueil (click on *Remonter le temps* and *Les prises de vues aériennes*)
1951	Les Houches. St-Gervais-les Bains N°4 Nord	Map	IGN	1:10 000	—
1959	IGNF_PVA_1-0__1959-09-09__C3530-0081_1959_FR166_0036	Aerial photograph	IGN	1:31 889	http://www.geoportail.gouv.fr/accueil (click on *Remonter le temps* and *Les prises de vues aériennes*)
1960	St-Gervais-les-Bains. Serie M 731. Feuille XXXV-31	Map	IGN	1:50 000	—
1977	St-Gervais-les-Bains. Serie M 731. Feuille 31-35	Map	IGN	1:50 000	—

of four 48*e* profiles), which starts in the upper slope. RO2 (B–C, 24*e*) extends the previous profile up to few metres above the steep front. RO3 (D–E, 48*e*) cuts the whole distal part of the Rognes area.

More contrasting electrical resistivities were measured than at Pierre Ronde. The upper slope (*c.* 250 m of length on RO1) displays resistivities >1000 kΩm directly under the coarse debris cover. The thickness of this resistive zone is hard to estimate because of the weak correlation between modelled and measured values in depth (very low MRMV). Below this 20 m deep zone, the resistivity decreases to 50 kΩm, possibly due to an inversion artefact in this poorly resolved model region. The central topographic depression consists of conductive materials (0.5 – 10 kΩm on RO1) in the whole investigated thickness (*c.* 40 m), except for a more resistive lens (10–50 kΩm, 10 m thick, 25 m long) located just before 320 m. In comparison with the top slope and the distal part, the better penetration of electric current in this conductive zone is expressed by the deepest location of MRMV thresholds. The distal part, visible on RO1, RO2 and RO3, shows a strong increase of resistivities in comparison with the central depression. Buried under 1 to 5 m thick conductive surface layer (<15 kΩm), a highly resistive body roughly 100 m wide and 30 m thick appears with values in the range 15–5000 kΩm. The weak correspondence of resistivity values at the crossing between RO1 and RO3 is probably due to inversion artefacts, expressed by very low MRMV (especially on RO1). Generally, but not systematically as shown by RO1, fine surface sediments are located above lower resistivity values.

Ground surface temperature (GST) measurements

Calculation of thermal indexes (MGST, WEqT and GFI) at 18 locations results in three main types of ground surface thermal behaviour (Figure 6A and Appendix A). The first one concerns all the sensors (1–7) located in the Rognes upper area. It is characterized by the coldest values obtained for the three indexes: MGST is between −2 and −4.4 °C, WEqT is between −4 and −5 °C, and GFI is < −750 °C day. The second type of thermal behaviour characterizes sensors 8 to 14, located downslope in the central and distal areas of Rognes, with intermediate values: MGST is between 0 and −2 °C, WEqT between −2 and −4 °C, and GFI between −250 and −750 °C day. Finally, the third type of behaviour is detectable for the sensors located in the Rognes marginal areas (sensors 15 and 16), in the upslope depression of Pierre Ronde (sensor 17) and in the southern side of the Rognes Ridge (sensor 18): MGST is positive, WEqT is between −0.6 and −2.1 °C, and GFI is > −600 °C day. The spatial distribution of these three types of behaviour outlines different thermal characteristics in the Rognes upper slopes, the Rognes central area, and the marginal and downslope sectors. Moreover, the vicinity of sensors 7, 8, 9, 10 and 15 suggests clear spatial limits between index values instead of progressive changes. It might indicate an important control of ground ice content and depth on ground surface temperatures.

Mean daily temperatures for four sensors are displayed in parallel with air temperature and snow cover from Météo France data (Figure 6B). Three different periods can be identified. First, there are daily temperature fluctuations, noticeably in the autumn, related to air temperature. The warm summer ground is freshened by cold air during this period, which can be trapped in the ground interstices. November corresponds to a frozen period for all sensors. This whole phase is attenuated for sensor 4, probably because of an early snow cover related to its elevation and slope aspect. The second period corresponds to the stabilization of ground surface temperature in winter under snow cover. The insulation of the ground from

atmosphere by the thickening of snow mantle between late November and early January (earlier than in ARMS data because the studied sites are located higher) is expressed by the slight rise in ground temperature curves (the heat transfer from the upper ground layers takes over the cold autumn air temperature influence) and its stabilization between January and mid April. Sensors 4 and 8 have the coldest WEqT (around −4 °C) and sensors 14 and 17 have a similar behaviour with a WEqT at −2.1 °C. Finally, the temperature rises rapidly to 0 °C for all sensors in May, in relation to the rise of air temperature and the moistening of snow cover; it occurs later for sensor 4 because of its elevation and aspect. This phase lasts during the whole melting of the snow mantle, which is not achieved in late June for all sensors. These temperature curves indicate that the ground surface experiences warmer conditions toward the distal part of Rognes. Sensor 17 at Pierre Ronde has higher values in autumn (a few days below 0 °C before mid-November) than in the low part of Rognes (sensor 14), but a similar WEqT.

Differential GPS measurements

Only a few small movements have been picked-up at Pierre Ronde (Figure 7). Eighteen boulders moved less than 5 cm (i.e. the precision threshold) in all calculated fields. Displacements up to 10 cm (Hm and Vm) only affected two boulders in the upper area and four boulders in the distal one. Movements have heterogeneous directions and most of them do not correspond with the slope direction.

Movements in Rognes are significant in both vertical and horizontal components (Figure 7). The Δv is < -25 cm for two-thirds of the 63 points, expressing an important generalized surface lowering. Four heterogeneous kinematic behaviours affecting specific sectors can be roughly distinguished. First, the upper area (10 points in the upper slope and associated footslope) is characterized by the highest values: Hm >50 cm, Vm and $\Delta v < -50$ cm. The movement direction is well correlated with the slope aspect. Significant surface kinematics particularly affects the terrain near 2850 m a.s.l., with displacements (Hm, Vm, Δv) >1 m. Second, the southwest margin up to the left area of the front (25 points) mostly displays homogeneous displacements: Hm between 10 and 50 cm, Vm between −10 and −50 cm, and Δv between −5 and −25 cm. The movement direction is to the north (direction of the central depression) for most of the boulders except for the five boulders of the front, which are oriented to the west (i.e. the slope aspect). Third, the north margin and the central depression (22 points) display contrasted direction and movements (Hm from 0 to 50 cm, Vm from −50 to 5 cm); six boulders moved <5 cm and Δv is always > -25 cm. Finally, in the right part of the front, west-southwest movements are mostly homogeneous (Hm between 10 and 50 cm, Vm between −5 and −50 cm, and Δv between +5 and −25 cm).

Interpretation of current ground ice distribution

The main landforms and the probable distribution of ground ice were mapped according to our observations and field measurements (Figure 8). Those results, which are all rather coherent, outline a different situation between Pierre Ronde and Rognes, whose origin and influence on sediment transfer are examined and discussed in the following section.

In the Pierre Ronde upper depression and southwest side of the distal slope, ground resistivity values are homogeneous, mostly in the range 2–10 kΩm in the total investigated depth (Figure 5: PR1, PR2, PR3 and the west side of PR4). Thermal measurements of sensor 17 reveal relatively warm conditions that appear weakly favourable to ground ice occurrence (MGST =0.1 °C, WEqT = −2.1 °C and GFI = −289 °C day; Figure 6). In comparison with Rognes thermal data, the positive MGST and the limited number of frozen days in autumn in the central area of Pierre Ronde (Figure 6B) may be related to a lower elevation and to the westerly slope aspect. Surface kinematics is almost inactive in this area except some very weak subhorizontal movements with heterogeneous direction (Figure 7). Morainic material is colonized by small pioneer plant species. It contrasts with recent debris flow deposits located in the south of this area (Figure 8), which illustrate the local supply of water in the sediment store. These characteristics all express a very likely absence of ground ice in this area (122 000 m^2 = 44% of Pierre Ronde area; Table II and Figure 8). Although based on few field data, we can assume that three

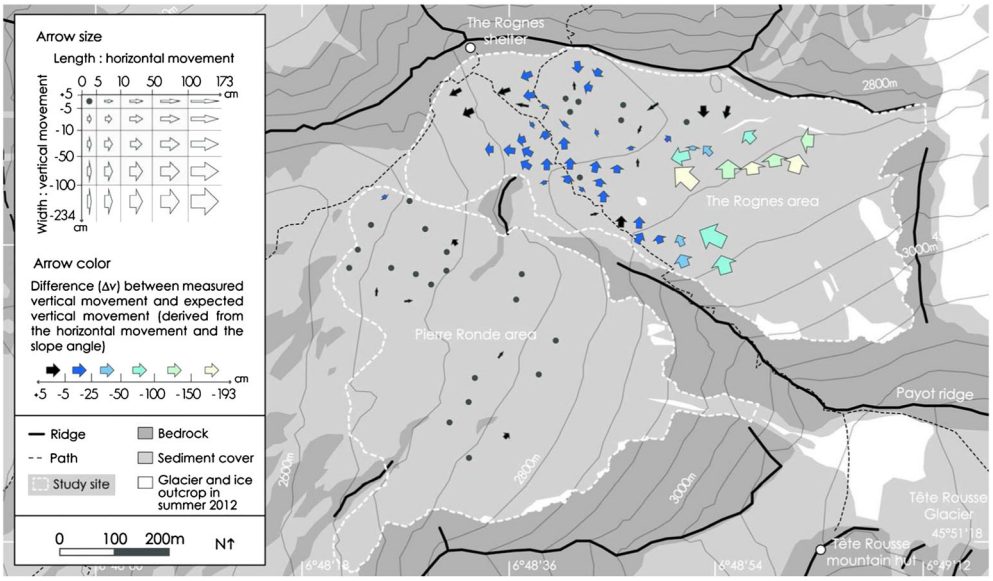

Figure 7. Movements measured with differential global positioning system (dGPS) in Rognes between 9 September 2011 and 28 August 2012 and in Pierre Ronde between 19 July and 3 October 2012. The slope angle used for the Δv calculation was determined with a 4 m-resolution digital elevation model (DEM) (source: RGD 73–74). This figure is available in colour online at wileyonlinelibrary.com/journal/espl

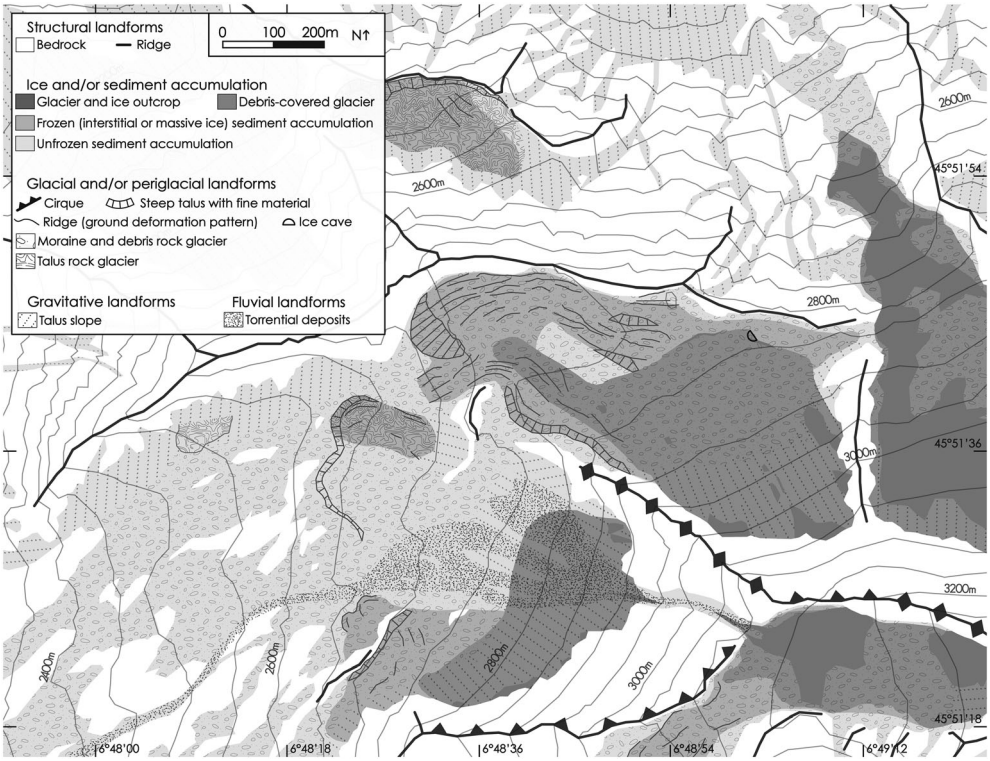

Figure 8. Simplified geomorphological map of Rognes and Pierre Ronde areas and ground ice distribution inferred from field observations and measured data (ERT, GST, DGPS).

other sectors of Pierre Ronde potentially contain ground ice (Figure 8). The upper slopes (one third of the total surface area; Table II) still probably contain an important amount of glacier ice. Even if no significant movements can be attributed to ice deformation or melt-out in this area during the Summer 2012 (Figure 7), our hypothesis is based on small ice outcrops and on the glacier evolution since the LIA (see later). The upper southwest side probably contains a frozen sediment zone, as suggested by some ground deformation patterns and a steep front with fine material. An important volume of massive ice might be present, as in the Rognes marginal frozen zone (see later and Figure 5). Finally, the northeast part of the distal zone shows typical features of a slightly active talus rock glacier: resistivity of 10 to 150 kΩm illustrating frozen sediments (PR4 on Figure 5), few deformation patterns (Figure 7), and a steep front with fine material. This area was probably not occupied by the glacier during the LIA and has probably evolved independently from glacial history in the last millennia.

The internal structure of Rognes differs noticeably from Pierre Ronde (Figure 8). Only the confined central depression (10 000 m^2 = 3% of the area; Table II) does not contain ground ice. The resistivity of this 200-m-long sector is mainly in the range 2–5 kΩm. Movements are limited at this smooth depressed surface partially covered by pioneer plant species (Figure 7). Thus, this sector can be considered as an unfrozen moraine. The upper slopes and a narrow tongue on the left side of Rognes entirely correspond to a debris-covered glacier occupying 57% of the total area (165 000 m^2; Table II). Massive ice is visible in many locations below the coarse-grained debris mantle. ERT, GST and dGPS data agree on glacier extent (resistivity >1000 kΩm; MGST < −2 °C; presumed WEqT < −4 °C and GFI < −750 °C day; Hm >50 cm, Vm and $\Delta v < -50$ cm). The maximal Δv values, reaching almost −2 m in the central and top slopes, suggest a rapid melt-out of the buried massive ice. By contrast, slower movements of the narrow northwest tongue (Figures 7 and 8) could result from the insulating effect of a few metre thick debris cover, as evidenced by the conductive top layer on RO3 (Figure 5). In the distal part, a frozen sediment zone surrounds the glacier and the central depression (Figure 8). Its surface, mostly convex, is dominated by coarse material; the many ridges, furrows and steep slopes with fine material give a chaotic topographical aspect to the sector. Resistivities of 10 to 500 kΩm suggest an ice-rich internal structure buried under a mean 3 m thick active layer. GSTs are higher than on the glacier (MGST > −2.3 °C; presumed WEqT > −4.5 °C and GFI > −750 °C day; Figure 6 and Appendix A). Surface kinematics is contrasted in term of values and direction, except for the boulders located in the northwest distal part where homogeneous westerly subhorizontal displacements have been pointed out (Hm in the range 10–50 cm; Figure 7).

Discussion

Glacier and ground ice evolution since the LIA

Based on (i) the hypothesized current ground ice distribution (Figure 8), (ii) the historical document analysis, and (iii) recent published data for the near Tête Rousse Glacier (cumulative mean specific net balance in Vincent *et al.* (2010); cold ice proportion in glacier volume in Gilbert *et al.* (2012)), we have reconstructed the evolution of both glacier and ground ice of the Pierre Ronde and Rognes since the last LIA maximum with 30-year steps (Figure 9). We describe and discuss here the main probable stages of this evolution.

First, at the LIA last maximum (locally *c.* 1820s; Vincent *et al.*, 2010), the Pierre Ronde Glacier was connected to the Tête Rousse Glacier (Figure 9a). Because of the deglaciated rockwall above it, Pierre Ronde Glacier was possibly partly debris-covered (Figure 9b), which could explain its absence in many historical sources. In contrast, the Rognes Glacier was most probably a bare-ice glacier connected to the Griaz Glacier. According to the many marginal deformation patterns of the northwest part (Figure 8), it was likely obstructed by

Table II. Geometrical characteristics of sediment accumulation in Rognes and Pierre Ronde. Mean sediment thickness and active layer thickness are inferred from field and measured data (ERT, GST, DGPS). The volume is roughly estimated with Equations (1) and (2) (see Methods) and given with a global error margin of 25% for the total volume of Rognes and Pierre Ronde areas

Sector	Area (m^2)	Area (%)	Estimated mean sediment thickness (m)	Estimated mean active layer thickness on frozen body (m)	Estimated sediment content in frozen body (%)	Estimated sediment volume (m^3)	Estimated volume (%)	Sediment volume/area ratio (m^3/m^2)
The Rognes area								
Glacier and debris-covered glacier	165 000	57	1	—	—	165 000	12	1
Marginal frozen body (debris rock glacier)	115 000	40	20	3	30	931 000 (345 000 + 586 000)	69	8.1
Unfrozen central depression	10 000	3	25	—	—	250 000	19	25
Total	290 000	100				1 346 000 (±336 000)	100	4.6
The Pierre Ronde area								
Glacier and debris-covered glacier	85 000	30	2	—	—	170 000	6	2
Upslope marginal frozen body (debris rock glacier)	49 000	17	15	3	30	323 000 (147 000 + 176 000)	12	6.6
Downslope marginal frozen body (talus rock glacier)	24 000	9	20	2	60	307 000 (48 000 + 259 000)	12	12.8
Unfrozen central slopes	122 000	44	15	—	—	1 830 000	70	15
Total	280 000	100				2 630 000 (±657 000)	100	9.4

pre-existing frozen sediments, and formed push moraines (western part of RO2 in Figure 5; Figure 9c). These glaciotectonically-deformed patterns result generally from glacier advances in permafrost environments (e.g. Etzelmüller and Hagen, 2005; Kneisel and Kääb, 2007). The elevation and aspect of the Rognes lower area are more favourable than at Pierre Ronde for the preservation of permafrost between Holocene glacier readvances (Table III). According to the maximal LIA extent of local glaciers, the ELA should have been around 2800 m. Therefore, without taking into account secondary ice supply by adjacent glaciers, the accumulation zone would have corresponded to the upper two-thirds of Rognes Glacier, but only to the upper one-third of Pierre Ronde Glacier (Figure 9a). Hence, the ratio between accumulation and ablation areas for the Pierre Ronde Glacier was lower than for bare-ice glaciers, as is typically the case for debris-covered glaciers (Ackert, 1998; Benn *et al.*, 2003).

Second, from the late LIA to about 1890, ice volume and extent likely remained large in both glaciers, reflecting the strong influence of LIA glacio-climatic conditions. The increase of debris cover on local glaciers during this period of dominant negative mass balance (Deline, 2005) was probably reduced on Rognes Glacier as rockfall activity was low due to a rockwall still noticeably ice-covered.

Third, for the period 1890–1950, we can assume that the Pierre Ronde supra-glacial debris cover was in part mobilized by the 1892 Tête Rousse WPOF (path in Figure 9a). An impervious ice layer under supra-glacial moraine facilitated their mobilization: water was maintained at the surface, saturating the debris cover and ice played the role of failure plane, as shown in recent events in the Italian Alps (Chiarle *et al.*, 2007). Thus, with the probable loss of the insulating debris cover (Figure 9b) and ice warming by water, negative mass balance in the decade would have accelerated Pierre Ronde Glacier shrinkage. After a period with positive or zero mass balance (1910–1930) and almost no debris cover on the Rognes Glacier (Figure 3B), significant negative mass balance in the 1940s, related to enhanced solar radiation and positive Atlantic Multidecadal Oscillation (Huss *et al.*, 2009; Huss *et al.*, 2010), led to rapid glacier wasting, as experienced by other glaciers in the Mont Blanc massif (Vincent *et al.*, 2010; Nussbaumer and Zumbülh, 2012). The thinning of ice has probably restricted Pierre Ronde Glacier in the upper depression (Figure 9c), whereas Rognes Glacier separated from the Griaz Glacier and became confined in its cirque. Like many glaciers unable to evacuate sediment load (Shroder *et al.*, 2000), both glaciers became mostly debris-covered. For this kind of glacier, the ablation gradient (i.e. the increase of melt rate toward glacier terminus in relation with rising of air temperature) can be inverted by an improved insulation of ice under a thickening debris layer in the distal area (Benn *et al.*, 2003; Hambrey *et al.*, 2008; Kellerer-Pirklbauer *et al.*, 2008). Maximal melt rate is experienced just below the ELA and the most distal and sheltered part is progressively disconnected from accumulation area (Benn *et al.*, 2012). This process can explain the situation in the Rognes area, where ice, protected by a thicker debris layer, has subsisted in the marginal parts and not in the central depression. In addition, a thinner snow cover in winter and meltwater surface runoff during summer could have increased the proportion of cold ice in the ablation area, whereas the ice in accumulation area is isolated from winter cold by the thick snow cover and warmed to the melting point by the release of latent heat when the meltwater refreezes in summer, as proposed for Tête Rousse Glacier (Gilbert *et al.*, 2012; Figure 9b). This process might explain the preservation and the progressive integration of cold glacier ice in the distal part of the Rognes area, in addition to pre-existent frozen sediments (Figure 9c). Thus polythermal glaciers are common in alpine or arctic permafrost environments (Etzelmüller and Hagen, 2005); their thermal regime explains the frequent glacier–permafrost interactions in the former lower and marginal areas whereas former central upper areas remain commonly unfrozen (Reynard *et al.*, 2003; Berger *et al.*, 2004; Kneisel and Kääb, 2007; Avian *et al.*, 2009; Ribolini *et al.*, 2010; Lilleøren *et al.*, 2013).

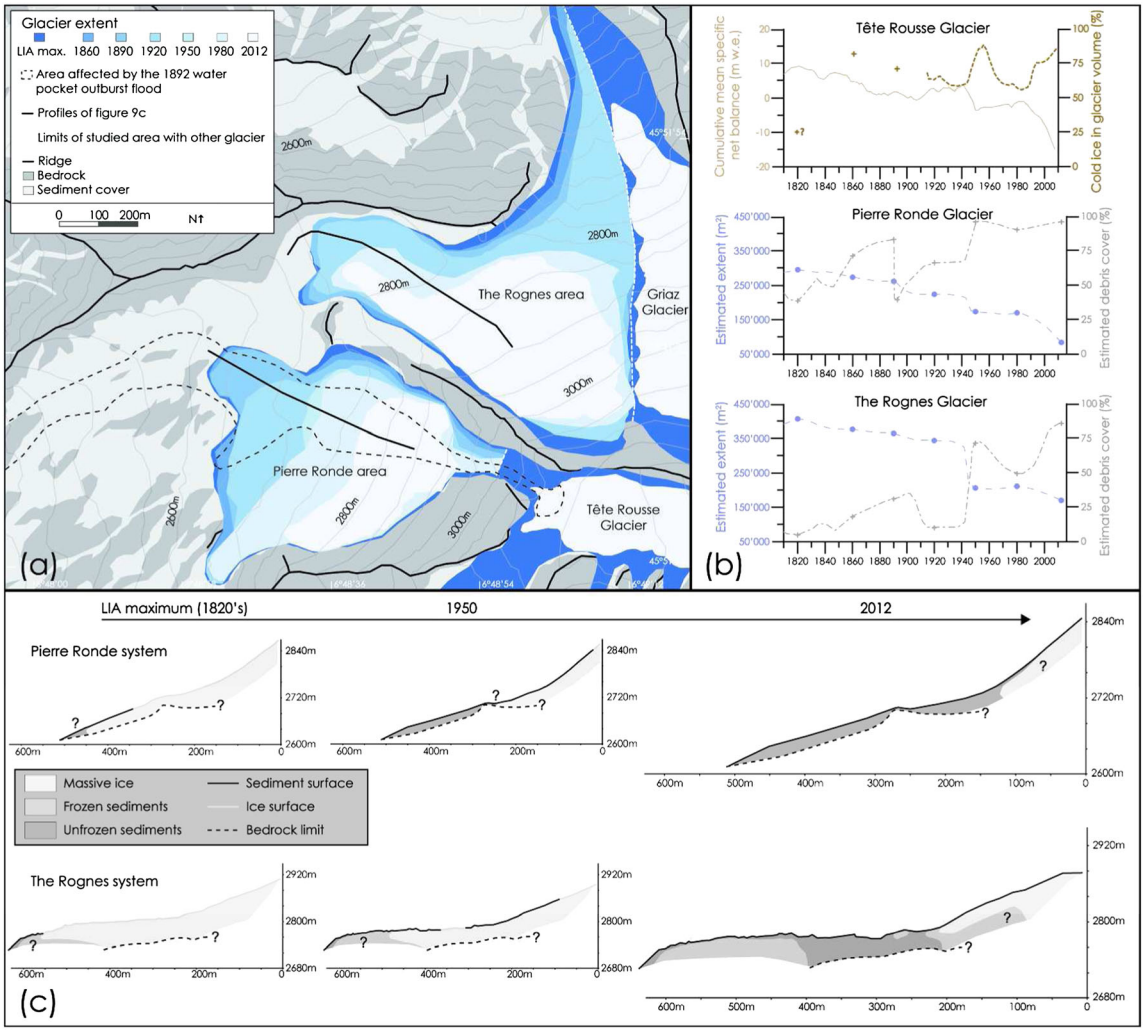

Figure 9. Evolution of Rognes and Pierre Ronde Glacier systems since the Litlle Ice Age (LIA) maximum. (a) Successive (30-year periods) extents of the studied glaciers. (b) Upper graph: recent cumulative mean specific net balance (synthetized from Vincent *et al.*, 2010) and ratio of cold ice in glacier volume (from Gilbert *et al.*, 2012) proposed for Tête Rousse Glacier. Combining these data with historical document analyses and proposed glacier extent in (a), we reconstructed the evolution of surface area (dots) and the ratio of debris cover (crosses) for Pierre Ronde and Rognes since 1820 (b: middle and lower graphs). Finally, (c) exposes longitudinal profiles of the studied areas for three different stages, following Figures 5, 9a and 9b data. This figure is available in colour online at wileyonlinelibrary.com/journal/espl

Table III. Topographical characteristics of the LIA maximal extent of Rognes and Pierre Ronde Glaciers derived from a 4-m-resolution DEM (from RGD 73–74)

Little Ice Age extent of:	Mean elevation (m a.s.l.)	Mean slope (deg)	Aspect (north/east/ south/west in %)	Mean direct solar radiation (Wh/m^2)
The Rognes glacier	2820	29.5	66.5/3/11.5/19	291 000
Pierre Ronde glacier	2760	27.5	9.5/1/8/81.5	289 000

Mass balance roughly stabilized between 1950s and mid-1980s (Figure 9b). We presume that the regional ELA was around 3000–3100 m, as it is located around 3200 m since the 1990s (Gilbert *et al.*, 2012). Thereby, the Rognes and Pierre Ronde Glaciers were almost completely below ELA and continued to shrink. However, glacier surface areas were nearly stable during these decades (Figure 9), probably due to the rapid and direct melt of glacier surface (downwasting) that contrasts with the delayed and complex variation of glacier length (Haeberli *et al.*, 2013). In this way, many glaciers have passed in the last decades from an active retreat dynamic to a progressive stationary thinning mode (Paul *et al.*, 2007; Hambrey *et al.*, 2008). It is especially the case for debris-covered glaciers (Scherler *et al.*, 2011; Deline *et al.*, 2012), where the glacier driving stress is weakened by the ice mass thinning and by the reduction of surface gradient that results from the inversion of the ablation gradient by the debris cover (Benn *et al.*, 2012). With this stationary thinning mode, ice caves development, due to sub- or intra-glacial water discharge and/or warm air circulation in summer, are common in ablation area (Haeberli *et al.*, 2013), as in the distal northeast limit of the Rognes area (Figure 3 and 8). With warm air penetration, the glacier melt-out is accelerated and can generate collapse structures.

Since the mid-1980s, mass balance has become extremely negative for local glaciers (Vincent *et al.*, 2010; Figure 9b). Despite extensive debris cover, warming climate led to rapid ice melt-out and current contrasted ground ice extent between Rognes and Pierre Ronde (Figures 8 and 9). This contrast most probably results from: (i) differences in elevation and aspect (Table III); (ii) the effect of the 1892 WPOF on Pierre Ronde debris cover; and (iii) repeated water supply by debris flows after 1892 in Pierre Ronde that led to a temperate thermal regime and hindering the formation of frozen sediment (Figures 5, 8 and 9), as it is commonly the case in areas covered by temperate glacier ice and affected by water circulation (Delaloye, 2004; Kneisel and Kääb, 2007; Ribolini *et al.*, 2010). In contrast, marginal areas seem to still contain ground ice (Table II

and Figure 8). Finally, a vanishing dead ice zone inherited from the LIA conditions occupies the upper slope of Pierre Ronde, where the shadow created by the rockwall and debris layer has limited ice melt. With a high rockfall activity, this sector can be interpreted as the first immature stage of talus slope development in a context of deglaciation (Gomez *et al.*, 2003). Rognes still contains a large amount of ground ice as pointed out by our field measurements (Figures 5, 6 and 7). The marginal frozen sediment zone is related to deformed pre-existent permafrost where cold massive ice of a polythermal glacier has been incorporated, a common situation in proglacial areas located in permafrost environments (Ackert, 1998; Reynard *et al.*, 2003; Etzelmüller and Hagen, 2005; Kneisel and Kääb, 2007). The relatively lower resistivity values (<5000 kΩm) in the northwest narrow glacier snout in comparison to the upslope debris-covered glacier (>5000 kΩm, Figure 5) and the moderate movements (Figure 7) suggest such transition from glacier ice to ice/debris mixture. The debris-covered glacier occupies an important surface area in the upper slopes. It can be also interpreted as a dead ice downwasting zone in transition to talus slope (Gomez *et al.*, 2003). The measured loss in elevation (Figure 7) between the GPS campaigns and the current meltwater circulation at the front of the Rognes Glacier suggest a probable domination of temperate ice.

Sediment transfer systems

According to our rough estimation of sediment volume (Table II), the store in Pierre Ronde (*c.* 2.6 Mm^3) appears to be twice that of the Rognes one (*c.* 1.3 Mm^3). This contrast might result from the intense frost weathering that affected non-glaciated Pierre Ronde rockwalls during the Holocene cold periods. Sediment volume/area ratio is 4.6 and 9.4 at Rognes and Pierre Ronde, respectively (Table II). The ratio of 11.8 for glacier forefield and 12–17 for hanging valley subsystems proposed by Otto *et al.* (2009) in the 75 km distant Turtmanntal (Switzerland) suggests that our estimation is realistic and might be slightly underestimated (especially in relation to our mean sediment thickness values).

The major sediment supply in the studied systems is the rockfall activity from the dominant fractured rockwalls (Figure 10). Permafrost degradation and/or intensification of freeze–thaw cycles might have led to an increasing activity of this process since the LIA (Deline *et al.*, 2012). With a negative mass balance, glaciers have been quite rapidly buried under debris (Figure 9b) as in other high relief contexts. The 1949 and 1959 aerial photographs (Table I) and field observations show that debris flow deposits filled the upper depression in Pierre Ronde (Figure 8). Their frequency is difficult to evaluate, although it appears low with some events per century, and some thousands of m^3 per debris flow (J. Lievois, Service Restauration des terrains en montagne of Haute-Savoie, personal communication). Since the recent formation of a new water pocket in Tête Rousse Glacier (Vincent *et al.*, 2012), a major local issue concerns the potential mobilization of Pierre Ronde sediments by an outburst flood: as revealed by ERT profiles (Figure 5), the central part of Pierre Ronde is composed of several metres of unconsolidated glacigenic sediments.

The reworking of the current sediment store within the studied area is the consequence of three main dynamics and is clearly related to ground ice occurrence (Figure 10). First, the debris-covered glacier sectors are the most active. The dynamics typical of almost stationary vanishing debris-covered glacier are occurring (Paul *et al.*, 2007; Schomacker, 2008; Benn *et al.*, 2012): massive ice melt-out, ice deformations, landslides on ice layer, ice cave formation. Movements can exceed 1 m/yr (Figure 7). Second, the weaker movements in frozen sediment areas are related to downslope creeping of ice/debris mixture. A thicker debris layer better insulates ground ice than in the upper slopes, as illustrated by lower Δv values. In addition to compressive patterns related to glacier advance, ice/debris mixture creeping generates the successive ridges and furrows and the steep front that are not visible in debris-covered glacier sectors. In this way, the active margins of Rognes and Pierre Ronde correspond to rock glaciers, defined as 'the visible expression of cumulative deformation by long-term creep of ice/debris mixtures under permafrost conditions' (Berthling, 2011, p. 103). Our results support the

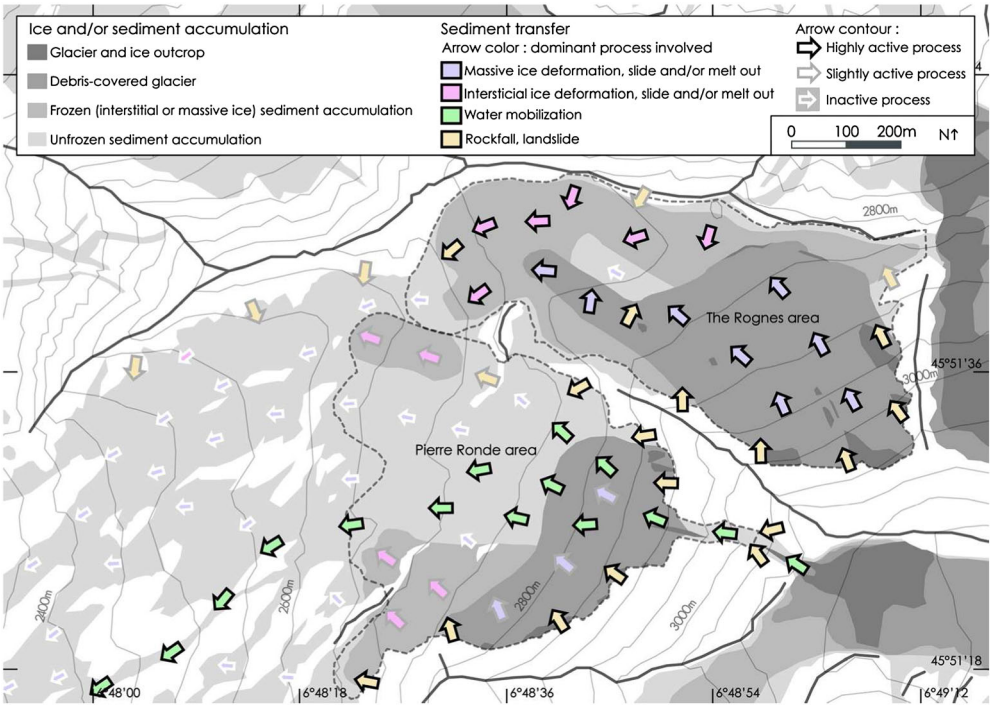

Figure 10. Schematic map on current sediment transfer in the Rognes and Pierre Ronde areas. The main geomorphic processes involved and their degree of activity are figured. This figure is available in colour online at wileyonlinelibrary.com/journal/espl

numerous studies on the glacier-rock glacier continuum that occurs in a negative mass balance context in permafrost environments (e.g. Ackert, 1998; Brazier *et al.*, 1998; Benn *et al.*, 2003; Krainer and Mostler, 2006; Avian *et al.*, 2009; Lilleøren *et al.*, 2013). Third, movements on the sides of the Rognes central depression can be interpreted as post-glacial re-equilibration as shown in other central areas of proglacial margins (Reynard *et al.*, 2003). The weak displacements in unfrozen sectors illustrate the limited mass wasting of sediments (Figure 10).

Figure 10 shows a conceptual map of sediment transfers in the studied areas and on the nearby slopes. Activity is mainly limited to Rognes and Pierre Ronde areas. Thus, we agree with other studies (e.g. Otto *et al.*, 2009; Carrivick *et al.*, 2013) that areas affected by glacial recession (even those with inherited ground ice) should be considered as some of the most dynamic parts of cold region geomorphic systems. However, as Pierre-Ronde and Rognes are not connected to downslope hydrosystems (any permanent surface runoff connects the studied sites downstream), this activity is mainly restricted to sediment store reworking within LIA glacier extents, and these sites can be considered as transport-limited systems and sediment sinks. Several complementary reasons, common in hanging valleys and glacier cirques, explain the decoupling of the studied areas from the sediment transfer system (Shroder *et al.*, 2000; Benn *et al.*, 2003). First, the bedrock topography inherited from the last glaciation has a relatively gentle slope (cirque floor) that has been progressively filled by sediments. Contributing to the reduction of relief energy, the current geometry of sediment accumulation (see the weakness of the slope angle on the ERT profiles on Figure 5) also contributes to the sediment trapping. Second, associated with this low relief energy, Holocene glacier and post-glacial processes had limited capacity to transfer sediment. Downstream sediment transport only occurred when the northeast tongue of the Rognes Glacier was coalescent with the Griaz Glacier, during the Tête Rousse WPOF, and with debris flows in the Pierre Ronde area. Finally, the moraine dam and/or marginal ice/debris mixture have contributed to the confinement of glaciers (the west tongue of Rognes Glacier), enhancing sediment stores. Therefore massive sediment stores have accumulated during the Holocene by successive glacier and post-glacial dynamics as in other decoupled glacier systems (Benn *et al.*, 2012). Thus, even if proglacial areas are particularly active in a paraglacial context, their contribution to sediment flux can be episodic rather than constant, in function of the capacity of geomorphic process to evacuate the sediment load downstream. This capacity can be strongly (sometimes completely) limited by the topography: glacier erosion and/or sediment accumulation geometry can generate sediment sinks. It is particularly frequent in the very numerous low active and small glacier systems (Brazier *et al.*, 1998; Shroder *et al.*, 2000; Benn *et al.*, 2003) and typically like the two study cirque glacier systems, where conjugate effects of low energy relief and limited capacity of Holocene geomorphic processes (even glacial transfer) have contributed to the formation of hypertrophic sediment stores. This situation is exacerbated in permafrost environment, when a distal ice/debris mixture (as in the Rognes area) obstructs the sediment transfer (Ackert, 1998; Brazier *et al.*, 1998; Berger *et al.*, 2004; Etzelmüller and Hagen, 2005; Krainer and Mostler, 2006). In contrast, this situation is scarcer in proglacial areas of large valley glaciers where the coupling between glacier system and hydrosystem heighten the efficiency of sediment transfer (e.g. Meigs *et al.*, 2006). Nevertheless, major sediment sinks, as proglacial lakes and the marginal zones (lateral moraines and slopes) disconnected from the valley floor hydrosystem, can exist even in these highly active landsystems (Cossart and Fort, 2008; Geilhausen *et al.*, 2012; Carrivick *et al.*, 2013).

Conclusion

According to our field observations and data, historical documentary analysis and published glaciological data on a small neighbouring glacier, a novel integrated geomorphological study has been provided for two small cirque glacier systems located in the periglacial belt of the Mont Blanc Massif. Pierre Ronde Glacier was probably debris-covered at the end of the LIA, whereas Rognes Glacier has been progressively buried due to the rockwall deglaciation that intensified during the twentieth century. Our results outline three main contrasted situations in terms of glacier system evolution since the LIA, current ground ice distribution, and geomorphological dynamics.

First, in the upslope debris-covered glacier areas, significant surface downwasting occurs currently, indicating the rapid melt-out of an ice body close to the melting point. The global negative mass balance that has followed the LIA has led to the confinement of glacier in the top slopes, where a decimetre thick debris mantle covers now the inherited ice.

Second, surface deformation patterns (ridges and furrows, steep front) and measured movements illustrate the creep of the marginal ice/debris mixtures. These accumulations have probably crept continuously since the LIA, decoupled from the upslope shrinking glacier. The probable integration of glacier ice in these landforms may be related to the existence of cold ice in the distal part of polythermal glaciers in permafrost environments. In addition, the inversion of ablation gradient due to the debris cover preserves ground ice better than in the central and upper slopes, as revealed by a convex topography and lower Δv values. As well, it expresses the glacier–permafrost interactions and the morphogenetic continuum between a debris-covered glacier and a rock glacier in a context of negative mass balance in permafrost environment.

Third, the lower half of Pierre Ronde surface and the central zone of the Rognes, characterized by concave topography, patches of fine material, and pioneer vegetation, correspond to deglaciated, unconsolidated moraine accumulations. In Pierre Ronde, post-LIA torrential dynamics has contributed to the recovery of the moraines by debris flow deposits. Absence of ground ice in these areas is mainly related to the former temperate thermal regime of glaciers and to the local frequent water supply. The current very weak surface activity reflects the slow rebalancing of sediment mass that affects these areas recently deglaciated.

At the Holocene timescale, Pierre Ronde and Rognes areas can be considered as sediment sinks and transport-limited systems. Sediment transfer occurred rarely, for instance on the occasion of events like the 1892 WPOF. In this way, Holocene geomorphic activity, in spite of repeated glacier advance and recession cycles, is largely restricted to sediment production and deposition within the glacier systems. The decoupling of these landforms with downslope geomorphic systems is common in small low active glacier systems (as the numerous cirque glaciers systems): geomorphic processes are unable to evacuate sediment especially because of the flat topography. In permafrost environments as in the Rognes area, this situation can be enhanced because marginal ice/debris mixtures obstruct sediment transfer. In that way, these small, decoupled landsystems act as sediment traps, as well as potential sediment source (especially in Pierre Ronde with a potential new WPOF from Tête-Rousse) and water reservoirs at catchment scale; their global understanding is important in a context of intensified changing climate.

Acknowledgements—The authors would like to thank the following people and institutions for their precious help during field measurements and documentary research: S. Utz, B. Regamey, L. Grangier, N. Deluigi, V. Zuchuat, R. Bosson, E. Malet, H. Dyer, J.-M. Krysiecki, C. Barachet; J.-F. Couix (*Refude du Nid d'Aigle*); *Météo France* for data from Aiguilles Rouges and Aiguille du Midi stations; the *Tramway du Mont-Blanc* crew (in particular E. Adami); *Remontées Mécaniques des Houches* (in particular K. Gafanesch); *ONF-RTM74* (in particular B. Demolis, J. Lievois and A. Evans); *LGGE* (in particular C. Vincent); *the Municipality of Saint-Gervais-les-Bains*; F. Amelot (*Centre de la Nature Montagnarde, Sallanches*). This manuscript has been improved thanks to the precious critics and comments of S. Lane and N. Deluigi (*IDYST, UNIL*), D. Morche, S. McColl and T. Heckmann (special issue editing team) and two anonymous reviewers.

Appendix A

Mean ground surface temperature, presumed winter equilibrium temperature and ground freezing index obtained at 18 locations with ground surface temperature measurements between 10th September 2011 and 20th June 2012 in Rognes and Pierre Ronde areas. Background colours correspond to classification in Figure 6a.

Sensor number (location on Figure 6A)	Mean ground surface temperature (MGST, °C)	Presumed winter equilibrium temperature (WEqT, °C)	Ground freezing index (GFI, °C day)
1	−2.6	−4.2	−815
2	−4	—	−1320
3	−4.4	−5	−1308
4	−3.1	−4.4	−911
5	−3	−5	−907
6	−2.3	−4.5	−744
7	−2.9	−5	−1025
8	−1.9	−3.5	−720
9	−1.8	—	−684
10	−0.3	—	−351
11	−1.1	−2.8	−547
12	−1.1	−3.5	−557
13	−0.9	—	−439
14	−1.2	−2.1	−437
15	0	—	−600
16	0.1	−1.6	−230
17	0.2	−2.1	−289
18	0.4	−0.6	−120

References

Ackert RPJ. 1998. A rock glacier/debris-covered glacier system at Galena Creek, Absaroka Mountains, Wyoming. *Geografiska Annaler* **80A**: 267–276.

Avian M, Kellerer-Pirklbauer A, Bauer A. 2009. LiDAR for monitoring mass movements in permafrost environments at the cirque Hinteres Langtal, Austria, between 2000 and 2008. *Natural Hazards and Earth System Sciences* **9**: 1087–1094.

Ballantyne CK. 2002. Paraglacial geomorphology. *Quaternary Science Reviews* **21**: 1935–2017. DOI. 10.1016/S0277-3791(02)00005-7

Barsch D. 1996. *Rock-glaciers – Indicators for the Present and Former Geoecology in High Mountain Environments*. Springer-Verlag: Berlin.

Benn DI, Kirkbride MP, Owen LA, Brazier V. 2003. Glaciated valley landsystems. In *Glacial Landsystems*, Evans DJA (ed.). Arnold: London; 372–406.

Benn DI, Bolch T, Hands K, Gulley J, Luckman A, Nicholson LI, Quincey D, Thompson S, Toumi R, Wiseman S. 2012. Response of debris-covered glaciers in the Mount Everest region to recent warming, and implication for outburst flood hazards. *Earth-Science Reviews* **114**: 156–174. DOI. 10.1016/j.earscirev.2012.03.008

Berger J, Krainer K, Mostler W. 2004. Dynamics of an active rock glacier (Ötzal Alps, Austria). *Quaternary Research* **62**: 233–242. DOI. 10.1016/j.yqrs.2004.07.002

Berthling I. 2011. Beyond confusion: Rock glaciers as cryo-conditioned landforms. *Geomorphology* **131**: 98–106. DOI. 10.1016/j.geomorph.2011.05.002

Bosson JB. 2012. Les glaciers enterrés du vallon des Jovet. *Nature et Patrimoine en Pays de Savoie* **38**: 16–23.

Brazier V, Kirkbride MP, Owens IF. 1998. The relationship between climate and rock glacier distribution in the Ben Ohau Range, New Zealand. *Geografiska Annaler* **80A**: 193–207.

Burger KC, Degenhardt JJJ, Giardino JR. 1999. Engineering geomorphology of rock glaciers. *Geomorphology* **31**: 93–132.

Carrivick JL, Geilhausen M, Warburton J, Dickson NE, Carver SJ, Evans AJ, Brown LE. 2013. Contemporary geomorphological activity throughout the proglacial area of an alpine catchment. *Geomorphology* **188**: 83–95. DOI. 10.1016/j.geomorph.2012.03.029

Chiarle M, Iannotti S, Mortara G, Deline P. 2007. Recent debris flow occurrences associated with glaciers in the Alps. *Global and Planetary Change* **56**: 123–136. DOI. 10.1016/j.gloplacha.2006.07.003

Cossart E, Fort M. 2008. Sediment release and storage in early deglaciated areas: towards an application of the exhaustion model from the case of Massif des Ecrins (French Alps) since the Little Ice Age. *Norsk Geografisk Tidsskrift – Norwegian Journal of Geography* **62**(2): 115–131. DOI. 10.1080/00291950802095145

Cuffey KM, Paterson WSB. 2010. *The Physics of Glaciers*. Elsevier: Amsterdam.

Delaloye R. 2004. Contribution à l'étude du pergélisol de montagne en zone marginal, PhD Thesis. GeoFocus 10. Département de Géosciences, Université de Fribourg.

Deline P. 2005. Change in surface debris cover on Mont-Blanc massif glaciers after the 'Little Ice Age' termination. *The Holocene* **15**: 302–309. DOI. 10.1191/0959683605hl809rr

Deline P, Gardent M, Magnin F, Ravanel L. 2012. The morphodynamics of the Mont Blanc massif in a changing cryosphere: a comprehensive review. *Geografiska Annaler* **94A**: 265–283. DOI. 10.1111/j.1468-0459.2012.00467.x

Etzelmüller B, Hagen JO. 2005. Glacier–permafrost interaction in Arctic and alpine mountain environments with examples from southern Norway and Svalbard. In *Cryospheric systems: Glaciers and Permafrost*, Harris C, Murton JB (eds), Special publications 242. Geological Society: London; 11–27.

Frey PA. 1988. *E. Viollet-le-Duc et le massif du Mont-Blanc, 1868–1879*. Payot: Lausanne.

Gardent M, Rabatel A, Dedieu JP, Deline P. 2014. Multitemporal glacier inventory of the French Alps from the late 1960s to the late 2000s. *Global and Planetary Change* **120**: 24–37. DOI. 10.1016/j.gloplacha.2014.05.004

Geilhausen M, Otto JC, Schrott L. 2012. Spatial distribution of sediment storage types in two glacier landsystems (Pasterze & Obersulzbachkees, Hohe Tauern, Austria). *Journal of Maps* **8**(3): 242–259. DOI. 10.1080/17445647.2012.708540

Gilbert A, Vincent C, Wagnon P, Thibert E, Rabatel A. 2012. The influence of snow cover thickness on the thermal regime of Tête Rousse Glacier (Mont Blanc range, 3200 m a.s.l.): consequences for outburst flood hazards and glacier response to climate change. *Journal of Geophysical Research* **117**: 165–182. DOI. 10.1029/2011JF002258

Gomez A, Palacios D, Luengo E, Tanarro LM, Schulte L, Ramos M. 2003. Talus instability in a recent deglaciation area and its relationship to buried ice and snow cover evolution (Picacho des Veleta, Sierra Nevada, Spain). *Geografiska Annaler* **85A**(2): 165–182. DOI. 10.1111/1468-0459.00196

Haeberli W. 2005. Investigating glacier–permafrost relationships in high-mountain areas: historical background, selected examples and research needs. In *Cryospheric Systems: Glaciers and Permafrost*, Harris C, Murton JB (eds), Special publications 242. Geological Society: London; 29–37.

Haeberli W, Hallet B, Arenson L, Elconin R, Humlum O, Kääb A, Kaufmann V, Ladanyi B, Matsuoka N, Springman S, Vonder MD. 2006. Permafrost creep and rock glacier dynamics. *Permafrost and Periglacial Processes* **17**: 189–214. DOI. 10.1002/ppp.561

Haeberli W, Huggel C, Paul F, Zemp M. 2013. Glacial responses to climate change. In *Treatise on Geomorphology*, Shroder JF (chief ed.),

James LA, Harend CP, Clague JJ (eds). Academic Press: San Diego, CA; 152–175.

Hambrey MJ, Quincey DJ, Glasser NF, Reynolds JM, Richardson SJ, Clemmens S. 2008. Sedimentological, geomorphological and dynamic context of debris-mantled glaciers, Mount Everest (Sagarmatha) region, Nepal. *Quaternary Science Reviews* **27**(25–26): 2361–2389. DOI. 10.1016/j.quascirev.2008.08.010

Hauck C, Kneisel C. (eds). 2008. *Applied Geophysics in Periglacial Environments*. Cambridge University Press: Cambridge.

Hausmann H, Krainer K, Brückl E, Mostler W. 2007. Internal structure and ice content of Reichenkar rock glacier (Stubai Alps, Austria) assessed by geophysical investigations. *Permafrost and Periglacial Processes* **18**: 351–367. DOI. 10.1002/ppp.601

Hilbich C, Marescot L, Hauck C, Loke MH, Mäusbacher R. 2009. Applicability of electrical resistivity tomography monitoring to coarse blocky and ice-rich permafrost landforms. *Permafrost and Periglacial Processes* **20**: 269–284. DOI. 10.1002/ppp.652

Huggel C, Clague JJ, Korup O. 2011. Is climate change responsible for changing landslide activity in high mountains? *Earth Surface Processes and Landforms* **37**: 77–91. DOI. 10.1002/esp.2223

Huss M, Funk M, Ohmura A. 2009. Strong alpine glacier melt in the 1940s due to enhanced solar radiation. *Geophysical Research Letters* **36**. DOI. 10.1029/2009GL040789

Huss M, Hock R, Bauder A, Funk M. 2010. 100-year mass changes in the Swiss Alps linked to the Atlantic Multidecadal Oscillation. *Geophysical Research Letters* **37**. DOI. 10.1029/2010GL042616

Ivy-Ochs S, Kerschner H, Maisch M, Christl M, Kubik P, Schlüchter C. 2009. Latest Pleistocene and Holocene glacier variations in the European Alps. *Quaternary Science Reviews* **28**: 2137–2149. DOI. 10.1016/j.quascirev.2009.03.009

Kääb A, Reynolds JM, Haeberli W. 2005. Glacier and permafrost hazards in high mountains. In *Global Change and Mountain Regions – A State of Knowledge Overview*, Huber UM, Bugmann HKM, Reasoner MA (eds). Springer: Berlin; 225–234.

Kellerer-Pirklbauer A, Lieb GK, Avian M, Gsurning J. 2008. The response of partially debris-covered valley glaciers to climate change: the example of the Pasterze Glacier (Austria) in the period 1964 to 2006. *Geografiska Annaler* **90A**(4): 269–285. DOI. 10.1111/j.1468-0459.2008.00345.x

Kneisel C. 1999. Permafrost in Gletschervorfeldern. Eine vergleichende Untersuchung in den Ostschweizer Alpen und Nordschweden, PhD Thesis. Trierer Geographischen Studien 22, Trier.

Kneisel C, Kääb A. 2007. Mountain permafrost dynamics within a recently exposed glacier forefield inferred by a combined geomorphological, geophysical and photogrammetrical approach. *Earth Surface Processes and Landforms* **32**: 1797–1810. DOI. 10.1012/esp.1488

Krainer K, Mostler W. 2006. Flow velocities of active rock glaciers, Austrian Alps. *Geografiska Annaler* **88A**: 1–14.

Krysiecki JM, Garcia S, Schoeneich P, Echelard T, Bodin X, Evans A. (nd). In preparation. D'un possible surge à la fin du 19ème siècle aux dynamiques actuelles: essai d'évaluation des vitesses moyennes de surface du glacier rocheux du Dérochoir sur 115 ans via la présence d'un chemin muletier.

Lambiel C, Delaloye R. 2004. Contribution of real-time kinematic GPS in the study of creeping mountain permafrost: examples from the western Swiss Alps. *Permafrost and Periglacial Processes* **15**: 229–241. DOI. 10.1002/ppp.496

Lilleøren KS, Etzelmüller B, Gärtner-Roer I, Kääb A, Westermann S, Gudmundsson A. 2013. The distribution, thermal characteristics and dynamics of permafrost in Tröllaskagi, Northern Iceland, as inferred from the distribution of rock glaciers and ice-cored moraines. *Permafrost and Periglacial Processes* **24**: 322–335. DOI. 10.1002/ppp.1792

Meigs A, Krugh WC, Davis K, Bank G. 2006. Ultra-rapid landscape response and sediment yield following glacier retreat, Icy Bay, southern Alaska. *Geomorphology* **78**: 207–221. DOI. 10.1016/j.geomorph.2006.01.029

Mennessier G, Rosset F, Bellière J, Dhellemmes R, Oulianoff N, Antoine P, Carme F, Franchi S, Stella A. 1976. *St-Gervais-les-Bains, Carte Géologique de la France à 1/50 000 703*. BRGM: Orléans.

Nussbaumer SU, Zumbülh HJ. 2012. The Little Ice Age history of the Glacier des Bossons (Mont Blanc massif, France): a new high-resolution glacier length curve based on historical documents. *Climatic Change* **111**(2): 301–334. DOI. 10.1007/s10584-011-0130-9

Otto JC, Schrott L, Jaboyedoff M, Dikau R. 2009. Quantifying sediment storage in a high alpine valley (Turtmanntal, Switzerland). *Earth Surface Processes and Landforms* **34**: 1726–1742. DOI. 10.1002/esp.1856

Owen LA, England J. 1998. Observations on rock glaciers in the Himalayas and Karakoram Mountains of northern Pakistan and India. *Geomorphology* **26**(**1–3**): 199–213. DOI. 10.1016/S0169-555X(98)00059-2

Owens PN, Slaymaker O. 2004. An introduction to mountain geomorphology. In *Mountain Geomorphology*, Owens PN, Slaymaker O (eds). Arnold: London; 3–29.

Paul F, Kääb A, Haeberli W. 2007. Recent glacier changes in the Alps observed by satellite: consequences for future monitoring strategies. *Global and Planetary Change* **56**: 111–122. DOI. 10.1016/j.gloplacha.2006.07.007

Reynard E, Lambiel C, Delaloye R, Devaud G, Baron L, Chapellier D, Marescot L, Monnet R. 2003. Glacier/permafrost relationships in forefields of small glaciers (Swiss Alps). *Proceedings of the 8th International Conference on Permafrost*, Zurich; Vol. 1, 947–952.

Ribolini A, Guglielmin M, Fabre D, Bodin X, Marchisio M, Sartini S, Spagnolo M, Schoeneich P. 2010. The internal structure of rock glaciers and recently deglaciated slopes as revealed by geoelectrical tomography: insights on permafrost and recent glacial evolution in the Central and Western Alps (Italy–France). *Quaternary Science Reviews* **29**: 507–521. DOI. 10.1016/j.quascirev.2009.10.008

Scapozza C. 2013. Stratigraphie, morphodynamique, paléoenvironnements des terrains sédimentaires meubles à forte déclivité du domaine périglaciaire alpin, PhD Thesis. Geovisions 40. Institut de géographie et durabilité, Université de Lausanne.

Scherler D, Bookhagen B, Strecker MR. 2011. Spatially variable response of Himalaysan glaciers to climate change affected by debris cover. *Nature Geoscience* **4**: 156–159. DOI. 10.1038/NGEO1068

Schomacker A. 2008. What controls dead-ice melting under different climate conditions? A discussion. *Earth-Science Reviews* **90**: 103–113. DOI. 10.1016/j.earscirev.2008.08.003

Serrano E, López-Martínez J. 2000. Rock glaciers in the South Shetland Islands, western Antarctica. *Geomorphology* **35**(1–2): 145–162. DOI. 10.1016/S0169-555X(00)00034-9

Shroder JF, Bishop MP, Copland L, Sloan VF. 2000. Debris-covered glaciers and rock glaciers in the Nanga Parbat Himalya, Pakistan. *Geografiska Annaler* **82A**(1): 17–31.

Stummer P, Maurer H, Green AG. 2004. Experimental design: electrical resistivity data sets that provide optimum subsurface information. *Geophysics* **69**(1): 120–139. DOI. 10.1190/1.1649381

Vaughan DG, Comiso JC, Allison I, Carrasco J, Kaser G, Kwok R, Mote P, Murray T, Paul F, Ren J, Rignot E, Solomina O, Steffen K, Zhang T. 2013. Observations: Cryosphere. In *Climate Change 2013: The Physical Science Basis. Contribution of Working Group I to the Fifth Assessment Report of the Intergovernmental Panel on Climate Change*, Stocker TF, Qin D, Plattner GK, Tignor M, Allen SK, Boschung J, Nauels A, Xia Y, Bex V, Midgley PM (eds). Cambridge University Press: Cambridge; 317–382.

Vincent C, Garambois S, Thibert E, Lefèbvre E, Le Meur E, Six D. 2010. Origin of the outburst flood from Glacier de Tête Rousse in 1892 (Mont Blanc area, France). *Journal of Glaciology* **56**(198): 688–698. DOI. 10.3189/002214310793146188

Vincent C, Descloitres M, Garambois S, Legchenko A, Guyard H, Gilbert A. 2012. Detection of a subglacial lake in Glacier de Tête Rouse (Mont Blanc area, France). *Journal of Glaciology* **58**(211): 866–878. DOI. 10.3189/2012JoG11J179